Article

Effect of Alkane Chain Length on Crystallization in Emulsions during Supercooling in Quiescent Systems and under Mechanical Stress

Serghei Abramov *, Kinza Shah, Lydia Weißenstein and Heike Petra Karbstein

Karlsruhe Institute of Technology (KIT), Institute of Process Engineering in Life Sciences (BLT), Section I: Food Process Engineering (LVT), Kaiserstr. 12, 76131 Karlsruhe, Germany; heike.karbstein@kit.edu (H.P.K.)

* Correspondence: serghei.abramov@kit.edu; Tel.: +49-721-608-42497

Abstract: Crystallization behavior of hexadecane ($C_{16}H_{34}$), octadecane ($C_{18}H_{38}$), eicosane ($C_{20}H_{42}$), and docosane ($C_{22}H_{46}$) dispersions of similar mean droplet diameter ($x_{50.2} \approx 15\ \mu m$) was investigated in quiescent systems and compared to crystallization under mechanical stress. In quiescent systems, the required supercooling decreased with increasing chain length of the alkanes to initiate crystallization. Crystallization of alkane dispersions under mechanical stress resulted in similar onset crystallization supercooling, as during quiescent crystallization. Increase of mechanical stress did not affect the onset crystallization supercooling within alkane dispersions.

Keywords: emulsion; dispersion; crystallization; melt emulsification; crystallization index; aggregation; nucleation

1. Introduction

Crystalline dispersions are widely used in chemical and life science industry [1–3]. They act as high performance lubricants or release agents, are applied as delivery systems with site-specific and controlled release kinetics or are added to foods and feeding stuffs to increase the bioavailability and biocompatibility of encapsulated active ingredients [4–10]. Due to distinctive viscoelastic behavior of the encapsulating material, these dispersions are usually produced in a two-step melt emulsification process: In the first step, the dispersed phase is emulsified above its melting temperature and transferred under supercooling into a fine crystalline dispersion in the second step [11–13].

During emulsification, molten bulk (dispersed phase) is homogenized to countless small volume units-the droplets. Different to bulk crystallization in a macroscopic volume element, crystallization in dispersed droplets occurs individually and separately in each droplet, resulting in polydisperse crystallization behavior during supercooling [14, 15]. The individual crystallization behavior in dispersions is strongly dependent on the formulation and process parameters, such as droplet size, additives, dispersed phase content, cooling rate, external forces and supercooling, as the driving force for crystallization in molten droplets [3, 9, 16–18]. Ideally, those parameters are adjusted to transform all droplets into spherical crystalline particles of the same size. Eventually, crystallization to different structures, incomplete crystallization and/or colloidal processes often occur during supercooling and destabilize the dispersions [19–24].

The final size, shape and physical state and thus the application properties of the dispersions are strongly connected to the nucleation within single droplets [25–28]. Usually, the formation of nuclei proceeds by heterogeneous nucleation mechanism due to catalytic impurities, which lower the nucleation barrier and allow crystallization at low supercooling [12]. In dispersions, the number of catalytic impurities is much lower than the number of droplets and require higher supercooling for crystallization compared to the bulk of the same material [3, 12]. The droplet size becomes a critical parameter for nucleation in dispersions as with increasing droplet size the probability of heterogeneous nucleation increases and crystallization becomes thermodynamically favorable [27,

45   29]. In most crystalline dispersions droplets are comparatively small (< 1 μm up to some μm) and the
46   size distribution is polydisperse. This causes incomplete crystallization depending on the
47   supercooling [14, 15].
48   In past decades, many researchers investigated crystallization in dispersed systems with focus
49   on the initiation of the nucleation. Different approaches, like surface-initiated, collision-mediated and
50   energy-induced nucleation were discussed [29–37]. One of the most promising approaches,
51   combining surface-initiated, collision-mediated and energy-induced nucleation, is stress-controlled
52   nucleation [15, 38–43]. Mechanical stress-induced crystallization is already industrially applied in
53   confectionery (chocolate) or dairy (whipped cream) industry to control and adjust morphology,
54   texture and mouthfeel [29, 43–47]. However, the impact of mechanical stresses on crystallization in
55   dispersed systems is still not fully understood and is a subject of many investigations.
56   In our previous investigations we discussed the individual and polydisperse crystallization in
57   hexadecane($C_{16}H_{34}$) dispersions [14] and the influence of rotation shear on the crystallization behavior
58   in hexadecane dispersions of different mean droplet size [15]. This current investigation expands the
59   homologous series by octadecane($C_{18}H_{38}$), eicosane($C_{20}H_{42}$), and docosane($C_{22}H_{46}$) dispersions and
60   focuses on the influence of oscillation mechanical stress, and discusses its impact on crystallization
61   intensification in dispersed systems.

62   **2. Materials and Methods**

63   *2.1. Materials*

64   All substances were commercially available and used as purchased without further purification
65   or processing. Hexadecane (HD, $C_{16}H_{34}$, purity 99%, melting point at 18°C) was purchased from
66   Sigma-Aldrich® (St. Louis, MO, USA). Octadecane (OD, $C_{18}H_{38}$, purity 99%, melting point at 28°C)
67   was purchased from Sigma-Aldrich® (St. Louis, MO, USA). Eicosane (EC, $C_{20}H_{42}$, purity 99%, melting
68   point at 37°C) was purchased from Sigma-Aldrich® (St. Louis, MO, USA). Docosane (DC, $C_{22}H_{46}$,
69   purity 95%, melting point at 44°C) was purchased from Sasol (Johannesburg, South Africa).
70   Polyoxyethylen-20-sorbitanmonolaurat (Tween®20) was purchased from Carl-Roth® (Karlsruhe,
71   Germany). Water was purified in a Milli-Q® instrument Q-POD® at 18.2MΩ (Darmstadt, Germany).

72   *2.2. Emulsion preparation*

73   Every emulsion consisted of 1wt% or 10wt% alkane (dispersed phase: hexadecane (HD),
74   octadecane (OD), eicosane (EC) or docosane (DC)), 1wt% Tween®20 (surfactant) and 98wt% or 89wt%
75   purified water (continuous phase). First, Tween®20 was dissolved under continuous stirring in
76   tempered purified water 10K above the melting temperature of the alkane ($\vartheta_{m,alkane}$) in a glass vessel.
77   Afterwards, the dispersed phase was added to the surfactant solution and tempered with the gear-
78   rim dispersing element (rotating part) for another 15min 10K above $\vartheta_{m,alkane}$ without stirring. Then,
79   the dispersed phase was homogenized with a gear-rim dispersing machine (IKA®T25 digital,
80   ULTRA-TURRAX®, Staufen im Breisgau, Germany) at 2.2m/s tangential speed (3,200rpm, 13mm
81   outer diameter of the rotating part) 10K above $\vartheta_{m,alkane}$ for 10min in a glass vessel of 25mm inner
82   diameter.
83   After emulsification, samples were taken for the quiescent crystallization (cryo-polarizing
84   microscopy of 1wt% emulsions) and crystallization under mechanical stress (oscillation mechanical
85   stress of 10wt% emulsions) analysis. Between emulsification and analysis, the emulsions were
86   continuously stirred above $\vartheta_{m,alkane}$ to avoid creaming, crystallization and inhomogeneous
87   sampling. During the sample preparation for the analytical part, emulsions did not show any sign of
88   instability.
89
90
91
92

93   *2.3. Droplet size distribution analysis*

94   The droplet size distributions (DSD) of emulsions were investigated using a customized
95   polarizing light microscope (Eclipse Ci-L, Nikon, Shinagawa, Tokyo, Japan) equipped with an
96   optically accessible temperature controlled stage (LTS 420, Linkam Scientific, Tadworth, UK).
97   After the emulsification, 25 µL of 1wt% alkane emulsions were pipetted between two
98   microscope cover slips glued on a tempered microscope object slide using tempered pipette, then
99   covered with a third cover slip and sealed with silicone 10K above $\vartheta_{m,alkane}$. Then, the sealed samples
100   were cooled to $\vartheta_{m,alkane}$ and equilibrated for 5min. Afterwards, images were taken of the emulsions
101   in liquid state. The obtained micrographs were processed with ImageJ 1.46r (National Institute of
102   Health, Bathesda, MD, USA) software to determine the characteristic values such as number, size and
103   size distribution by area of the emulsions. Details are given in [14].

104   *2.4. Quiscent crystallization analysis*

105   In analogy to DSD analysis, same thermo-optical equipment and sample preparation procedure
106   were applied to investigate quiescent crystallization behavior in alkane dispersions, as described in
107   chapter 2.3.
108   First, **onset crystallization temperature** and **melting temperature** of the dispersions were
109   determined, since these values are subject of Kelvin effect and might vary in dependency of mean
110   droplet size [48]. The samples were cooled to 18K (entire crystallization of all droplets within the
111   dispersion) supercooling with a cooling rate of 1K/min. During supercooling, picture sequences of
112   the crystallizing dispersions were taken every 0.2K. The onset crystallization temperature of the
113   dispersions was determined optically by the appearance of the first crystallized droplet (gray
114   transparent droplet→green opaque spheroid) in the volume. Then, the samples were re-heated to
115   10K above $\vartheta_{m,alkane}$ with a heating rate of 1K/min. During heating, picture sequences of the melting
116   dispersions were taken every 0.2K. The melting temperature of the dispersions was determined
117   optically by change of color and shape of the droplets (green opaque spheroids→gray transparent
118   droplets).
119   Influence of the **cooling rate** on crystallization in alkane dispersions was investigated by varying
120   the cooling rate. The samples were cooled to supercooling of 18K with a cooling rate $\Delta T/\Delta t$ of
121   0.1K/min, 1K/min and 10.0K/min. During supercooling, picture sequences of the droplets were taken
122   every 0.2K. Due to polarization the crystallized droplets change their color from gray transparent to
123   green opaque and can be easily differentiated from liquid droplets. The number of crystallized
124   droplets was optically followed in dependency of cooling rate.
125   To exclude the effect of **time dependency** during crystallization in alkane dispersions isothermal
126   observations were performed. Since the dependency of cooling rate on crystallization in alkane
127   dispersions decreased with increasing chain length (see appendix C, Figure C3), only HD dispersions
128   were investigated. HD samples were cooled to supercooling of 2.5, 4.5 and 8.5K and held at each
129   supercooling for one hour. During the isothermal observations, picture sequences of the droplets
130   were taken every 12s. Due to polarization the crystallized droplets change their color from gray
131   transparent to green opaque and can be easily differentiated from liquid droplets. The number of
132   crystallized droplets was optically followed in dependency of time.
133   The main objective of thermo-optical investigations was to describe and quantify the
134   crystallization behavior in alkane dispersions by determination of **crystallization index by number**
135   **CI$_N$** in quiescent systems. Similar to previous investigations, the alkane dispersion samples were
136   cooled to 18K supercooling with a cooling rate of 1K/min. During supercooling, picture sequences of
137   the crystallizing dispersions were taken every 0.2K. The obtained micrographs were processed with
138   ImageJ 1.46r (National Institute of Health, Bathesda, MD, USA) software to differentiate between
139   liquid and crystalline structures, to determine the characteristic values such as number, size and size
140   distribution of crystallized and supercooled droplets and to calculate the number based
141   crystallization index CI_N within the dispersions:

$$CI_N = \frac{N_{cr,p}}{N_d + N_p} \qquad (1)$$

142   Details of the thermo-optical method are shown in our earlier paper [14].

143   *2.5. Crystallization under mechanical stress*

144   Crystallization behavior of bulk alkane and alkane in water dispersions under oscillation
145   mechanical stress was investigated using a rotational rheometer (Physica MCR301, Anton Paar, Graz,
146   Austria) equipped with a double gap geometry DG26.7 in oscillation mode.
147   At this point, no rheological evaluation has been done yet. The rotational rheometer has been
148   merely used as a precise tempered shear cell. Only mechanical values, such as torque (M) as a signal
149   for crystallization, and deformation (γ) or frequency (f) as setting parameters to adjust oscillation
150   mechanical stress, have been used to describe the crystallization behavior under mechanical stress
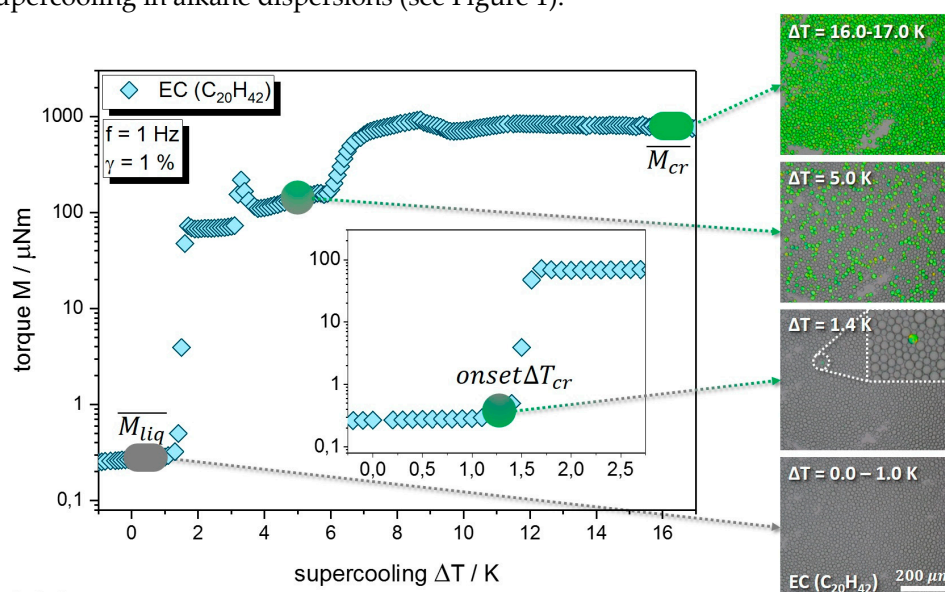151   during supercooling in alkane dispersions (see Figure 1).

152

Figure 1: Torque M as a function of supercooling at constant deformation γ of 1% and frequency f of 1Hz of
10wt% eicosane dispersion. Micrographs on the right are depicted results of quiescent crystallization (without
mechanical treatment).

156   Three major impacts on the torque during oscillation mechanical treatment are connected to the
157   supercooling of organic dispersions: (1) constant increase in torque due to supercooling (increase in
158   viscosity), (2) additional increase in torque due to crystallization/solidification of organic substances
159   (increase of inner friction due to solidification) and (3) crystallization/solidification driven
160   aggregation leading to fluctuation and further increase in torque (aggregate formation and breakage
161   processes, dependent on the mechanical stress).
162   **Sample preparation:** 3.8mL of 10wt% alkane emulsion were pipetted into the tempered
163   measuring cup using a tempered pipette 10K above $\vartheta_{m,alkane}$. The measuring bob was placed into
164   the gap and tempered with alkane emulsion for additional 5min 10K above $\vartheta_{m,alkane}$. To reduce
165   impurities/alien nuclei, the measuring geometry was washed with water, then isopropanol, and
166   afterwards dried for 5min in dust and lint free environment.
167   Impact of **mechanical stress** on crystallization: Samples of 10wt% alkane dispersion were cooled
168   to 18K supercooling with a cooling rate of 1K/min. During cooling three different deformations γ, 1,
169   100 and 10,000%, and three different frequencies f, 1, 10 and 100Hz, were applied. Deformation and
170   frequency are proportional in square to the dissipated energy during oscillation and were used to
171   vary the mechanical stress intensity during crystallization. To compare the torque within the
172   experimental series, normalized torque was calculated:

$$M_{norm} = \frac{M}{M_{max}} \tag{2}$$

173 Mechanical treatment is reported to accelerate nucleation and thus the crystallization progress
174 in dispersed systems [3, 49]. Acceleration of crystallization process can be identified by: (1) decrease
175 of required supercooling for crystallization and (2) increase of crystalline content. Therefore, we
176 determined the onset crystallization supercooling (supercooling, at which first crystallization effects
177 on torque were detected) and phase transition torque factor (quotient of torque after and before
178 crystallization) to compare the impact of mechanical stress intensity on crystallization behavior in
179 emulsions.

180 **Onset crystallization supercooling:** To determine the onset crystallization supercooling
181 *onset* ΔT_{cr} we evaluated the torque as function of supercooling and stress intensity. For this, we
182 determined the first significant increase in torque (over 10%) as a result of supercooling and
183 mechanical stress (see Figure 1, magnified diagram):

$$onset\ \Delta T_{cr}(M) = \Delta T\left(\frac{M_{i+1}}{M_i} \geq 1.1\right) \tag{3}$$

184 **Phase transition torque factor:** To estimate the crystallization progress in dispersions we
185 determined the phase transition torque M_{pht} in dependence of mechanical stress intensity.
186 Therefore, we calculated the mean torque $\overline{M_{cr}}$ between 16 and 17K supercooling (every droplet was
187 crystalline at this supercooling during quiescent crystallization in alkane dispersions) and related it
188 to the mean torque $\overline{M_{liq}}$ between 0 and 1K supercooling (every droplet was liquid at this
189 supercooling during quiescent crystallization in alkane dispersions):

$$M_{pht} = \frac{\overline{M_{cr}}}{\overline{M_{liq}}}$$

191 *2.6. Statistical analysis*

192 Every emulsion and every experiment was prepared/performed three times for triple
193 determination. Uncertainty was calculated using commercial software MATLAB R2017, Microsoft
194 Excel 2016 or Origin 2017 and expressed as standard deviation.

195 **3. Results and discussion**

196 *3.1. Quiscent crystallization*

197 Three parameters, droplet size (appendix A), melting point (appendix B) and time dependency
198 (appendix C) of crystallization behavior in alkane dispersions, were analyzed prior the determination
199 of crystallization index. Since these parameters were needed for the quiescent crystallization analysis,
200 but are not the main topic of our discussion, details are given in the appendix sections A-C.

201 During the thermo-optical observations of quiescent crystallization behavior in 1wt% alkane
202 dispersion three different physical states occurred: liquid droplets above melting temperature (grey,
203 transparent spheres), supercooled liquid droplets below melting temperature (grey, transparent
204 spheres) and poly crystalline structures below melting temperature (green, opaque spheroids). We
205 did not observe any amorphous structures (grey, opaque spheroids) or recrystallization to single
206 crystalline structures (colored, transparent polygons) due to low supercooling rate and short
207 experiment duration of 20min. Alkane droplets crystallized to poly crystalline spheroids and retained
208 nearly spherical (see Figure 2).
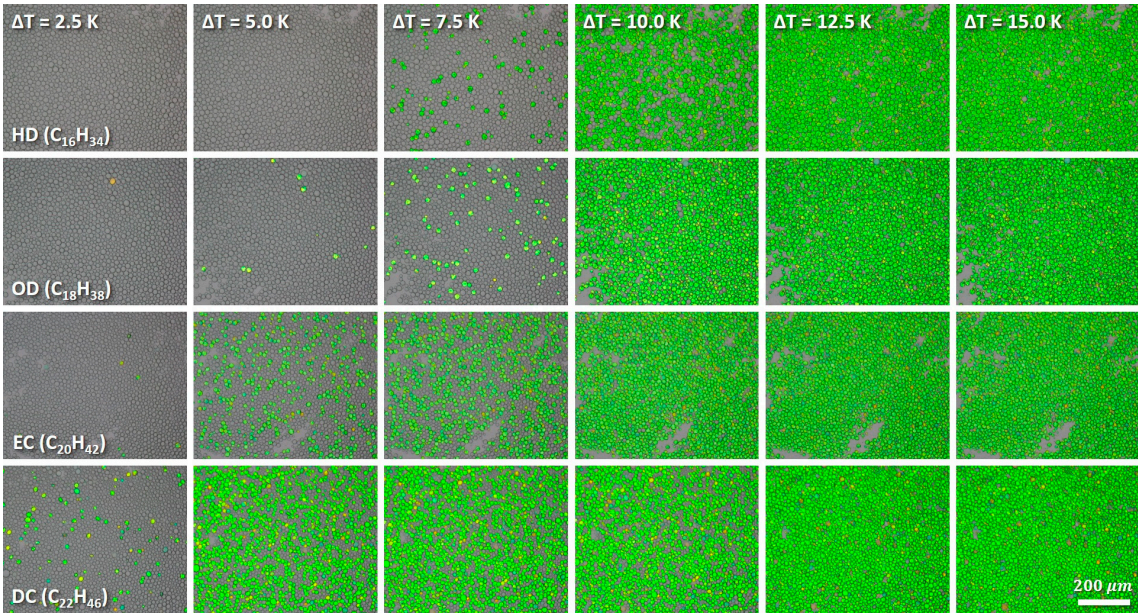
Figure 2: Micrographs of 1wt% alkane dispersions at different supercooling with a cooling rate of 1K/min. Length of the scale bar is 200 μm.

At low supercooling, droplets crystallized individually and stochastically distributed in the volume independent of their size. This crystallization behavior is connected to the impurity initiated crystallization, where impurities reduce the nucleation barrier in droplets and cause crystallization at relatively low supercooling [3, 49]. In emulsions, the volume of individual droplets is usually much smaller than the number of droplets. Therefore, crystallization in emulsion droplets containing no impurities requires higher supercooling and is strongly dependent on the droplet size. The general experience shows, that with increasing purity and decreasing droplet size high supercooling is required for nucleation in emulsions [3, 15].

Within the homologues series HD ($C_{16}H_{34}$), OD ($C_{18}H_{38}$), EC ($C_{20}H_{42}$) and DC ($C_{22}H_{46}$), we observed different crystallization behavior of droplets in dependence of the alkane chain length. Similar to onset crystallization temperature (appendix B), the onset crystallization supercooling decreased with increasing chain length of the alkanes. To quantify the crystallization progress in alkane dispersions, we calculated the crystallization index by number CI_N (see Figure 3).
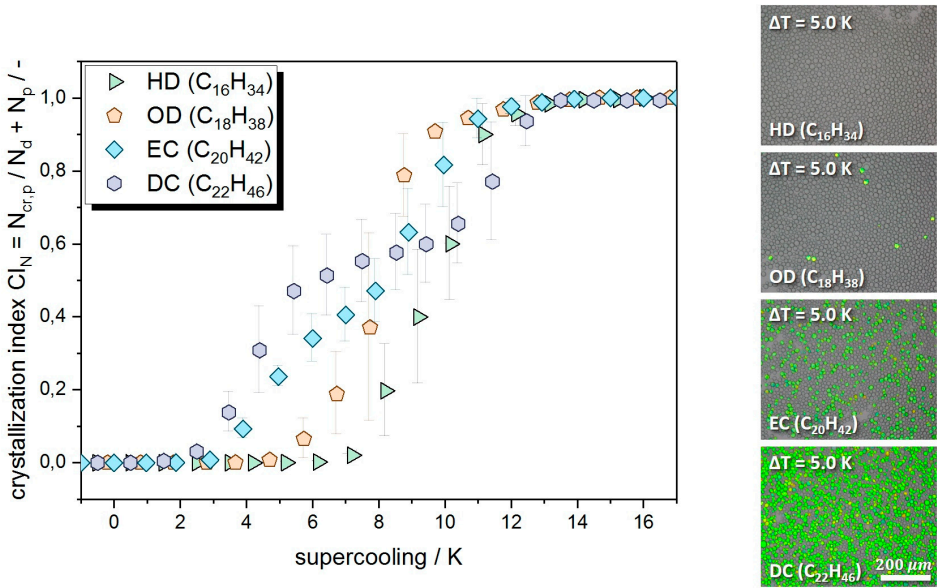

Figure 3: Number based crystallization index CI_N of 1wt% alkane dispersions as a function of supercooling ΔT with a cooling rate of 1K/min. Length of the scale bar is 200 μm.

In HD dispersions, crystallization index remained nearly zero at low supercooling and increased continuously and linear during further supercooling. At a critical supercooling ($\Delta T=12K$) all observed droplets crystallized. Similar to HD dispersions, crystallization index in OD dispersions increased continuously and linear, until complete crystallization of the droplets ($\Delta T=10.5K$). The crystallization index of EC dispersion showed nonlinear increase with a stagnation region (stagnation between 6 and 8K supercooling). In case of DC dispersions, the nonlinear behavior of the crystallization increased with a more pronounced stagnation region (stagnation between 5 and 10K supercooling). The stagnation during EC and DC crystallization indicates two different nucleation types, low nucleation barrier (crystallization at low supercooling, type I) before the stagnation and high nucleation barrier (crystallization at high supercooling, type II) [29, 49, 50]. Those stagnation regions might be the cause of impurities, different nucleation mechanisms or most likely formation of intermediate structures (polymorphism).

The chain length of investigated alkanes had a great influence on the crystallization progress in alkane dispersions, as shown in Figure 3 in micrographs on the right. At 5K supercooling alkane dispersions of similar mean droplet size showed different crystallization progress at the same formulation and process conditions: no crystallization in HD dispersions ($CI_{N,HD}=0.00$); OD dispersions crystallized to 1% ($CI_{N,OD}=0.01$); 24% of all droplets crystallized in EC dispersions ($CI_{N,EC}=0.24$); crystallization of 40% by number in DC dispersions ($CI_{N,DC}=0.40$).

3.2. Crystallization under mechanical stress

Different to direct number based observation of crystallization in previous chapter, torque was used as indirect integral signal to follow crystallization in alkane dispersions under mechanical stress. Liquid-solid phase transition, such as crystallization, is connected to an increase in inner friction or flow resistance during mechanical treatment. Therefore, crystallization under mechanical stress results in increased torque signal, which can be used as an indicator for crystallization events in dispersed systems [41–43].

Compared to the quiescent crystallization in chapter 3.1, alkane dispersions under low mechanical stress ($f = 1Hz$ and $\gamma = 1\%$) show similar trend in the start of crystallization: With increasing chain length the onset crystallization supercooling decreases in alkane dispersions (see Figure 4). However, the onset crystallization supercooling was equivalent within the standard deviation to quiescent crystallization behavior (see Figure 4, diagram on the right).
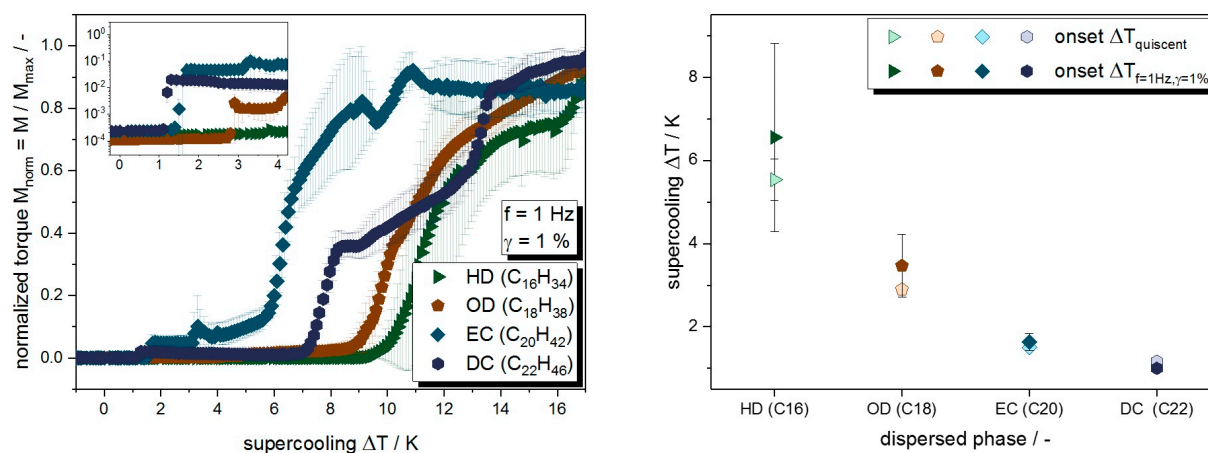

Figure 4: Left: Normalized torque M_{norm} of 10wt% alkane dispersions under low oscillation mechanical stress as a function of supercooling ΔT. Right: Comparison of onset crystallization supercooling during quiescent crystallization $onset\Delta T_{quiescent}$ and crystallization under low mechanical stress $onset\Delta T_{f=1Hz,\gamma=1\%}$.

Two general effects of non-destructive mechanical treatment might influence the crystallization in dispersed systems: (1) Energy input over the mechanical work connected to immobilization of molecules for nucleation [51] and (2) collision of moving droplets/particles in the flow field leading

266 to secondary nucleation [49]. Dissipated energy during oscillation mechanical stress treatment is
267 proportional in square to the frequency f and deformation γ and can be adjusted by these two
268 parameters. Theoretically, increasing the frequency at low deformation (such as 1%) mostly results
269 in energy input (effect 1) and increasing the deformation at low frequency (such as 1 Hz) mostly
270 results in flow field mediated collisions (effect 2). Therefore, we varied the frequency f at low
271 deformation and deformation γ at low frequency to observe the influence of mechanical stress on
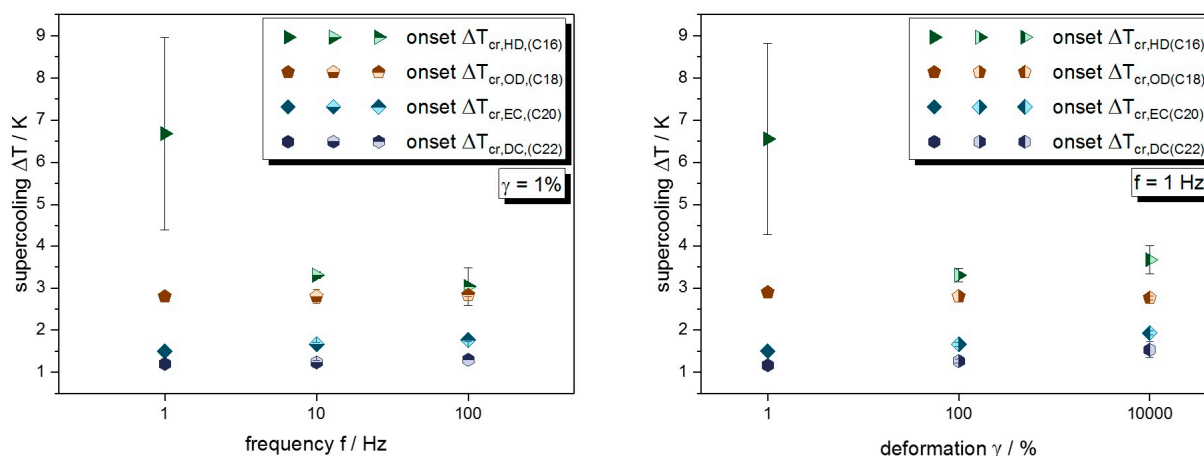272 the onset crystallization supercooling in alkane dispersions (see Figure 5).

273

274 Figure 5: Left: Onset crystallization supercooling of 10wt% alkane dispersions $onset\Delta T_{cr,dispersion}$.as a function
275 of frequency f. Right: Onset crystallization supercooling of 10wt% alkane dispersions $onset\Delta T_{cr,dispersion}$ as a
276 function of deformation γ.

277   In general, we observed no or only little influence of frequency or deformation during oscillation
278 mechanical stress on onset crystallization supercooling in alkane dispersions. Onset crystallization
279 supercooling tended to increase with increasing frequency and deformation and thus with increasing
280 mechanical treatment. According to the comparatively small increase, standard deviations and the
281 used analytical method, this might be also connected to the sensitivity of the method (no detection of
282 crystallization events on single droplet level, several crystallization events are required for detection).
283 The onset supercooling in dispersions represents only a small number of crystalline droplets. This
284 small number of droplets, which crystallized at low supercooling, might also crystallize according to
285 impurity-initiated mechanism and independent of mechanical treatment. However, the major
286 fraction of droplets in dispersions crystallizes at higher supercooling. Consequently, to describe the
287 crystallization progress in dispersions requires quantitative determination of crystallization index CI_i
288 as a function of mechanical stress over relevant supercooling range. Therefore, we evaluated the
289 crystallization progress in alkane dispersions by calculation of the phase transition torque factor (see
290 Figure 6), which takes the mean torque at high supercooling (between 16 and 17K, every droplet was
291 crystalline during quiescent crystallization analysis) into ratio to mean torque at low supercooling
292 (between 0 and 1K, every droplet was liquid during quiescent crystallization analysis). Since liquid-
293 solid phase transition causes higher flow resistance, dispersions with high crystallinity result in
294 increase of torque during mechanical treatment. Additionally, crystallizing droplets do not only
295 change their physical state but also form crystalline structures, which differ from the shape of
296 spherical droplets. Those crystalline structures provide more interactive surface, than point contact
297 of spheres and result in stronger aggregation due to van der Waals forces. During oscillation
298 mechanical treatment, aggregation results in supplementary increase in torque, in addition to the
299 increase due to supercooling and phase transition. Consequently, high torque transition factor
300 indicates high state of crystallinity and/or crystallization initiated aggregation in dispersed systems.
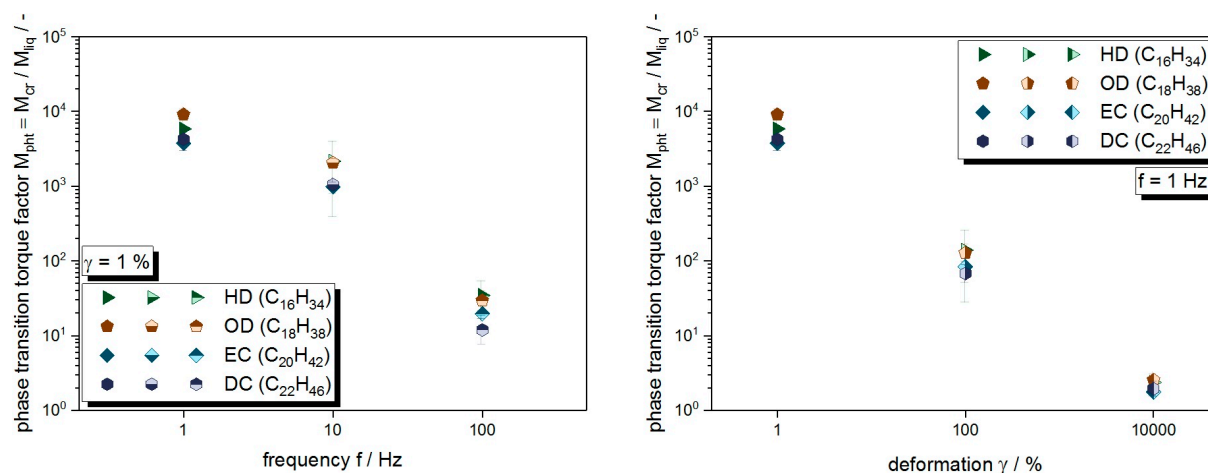
301

Figure 6: Left: Phase transition torque factor of 10wt% alkane dispersions M_{pht} as a function of frequency f.
Right: Phase transition torque factor of 10wt% alkane dispersions M_{pht} as a function of deformation γ.

At low frequency and low deformation, the phase transition torque factor was comparatively high in range of several thousand indicating advanced crystallization and/or crystallization dependent agglomeration in dispersions. Different to low mechanical stress during supercooling, we measured a decrease in phase transition torque factor by applying both, high frequencies or high deformations, indicating less flow resistance and consequently less crystallization and/or crystallization initiated aggregation. This was in contrary to the expectations, since mechanical treatment, especially at high deformation, increases the collision rates and therefore the secondary or collision-mediated nucleation in dispersions [3, 49].

At this point it should be noted, that two aspects are important for the efficiency of collision mediated nucleation: (1) collision frequency/probability, which increases with increasing mechanical treatment, and (2) collision time, which decreases with increasing mechanical stress. Therefore, there is a limit in mechanical stress, which is able to promote secondary nucleation in dispersions. This limit is the collision time. The collision time must be larger than the required time for colliding supercooled droplet to wet the surface of crystallized droplet in contact, and initiate secondary nucleation. Otherwise, mechanical treatment will result in frequent collisions without nucleation leading to low crystallinity in dispersions. In addition, from thermodynamic point of view, every energy input, such as work or heat during mechanical treatment, increases the free energy of the system and might inhibit the nucleation. Of course, this strongly depends on ability of the system to convert and save the energy in order to increase its overall energy.

Still, the increase in torque during supercooling cannot be clearly connected to crystallization or aggregation/aggregation-breakage effects separately using torque as an indicator for crystallization in the tempered shear cell. To identify the mechanisms of crystallization under mechanical stress requires a combination of optical, mechanical and thermal measuring method, and is a subject of our ongoing work.

4. Conclusions

Crystallization behavior of alkane dispersions with different chain lengths, hexadecane($C_{16}H_{34}$), octadecane($C_{18}H_{38}$), eicosane($C_{20}H_{42}$), and docosane($C_{22}H_{46}$), showed strongly chain length dependent crystallization behavior. With increasing chain length, the required supercooling and thus the driving force for the initiation of crystallization, decreased within the investigated alkanes. Unlike to the entire and instantaneous crystallization after nucleation in pure alkanes, crystallization in investigated alkane droplets occurred individually and stochastically distributed among the observed supercooling range. Different to hexadecane and octadecane dispersions, eicosane and docosane dispersions had a stagnation region within the crystallization process indicating two different nucleation types. At high critical supercooling (13K) and independent of the alkane chain length, every droplet crystallized within the investigated sample.

339   Appling mechanical stress during supercooling in alkane dispersions and following the
340 crystallization process by measuring the torque led to qualitatively similar crystallization behavior,
341 as in quiescent systems. Mechanical stress did not affect the required supercooling for initiation of
342 crystallization process. Consequently, increase of frequency or deformation during oscillation
343 mechanical treatment led to similar onset crystallization supercooling. Increase of mechanical stress
344 caused unexpected decrease in torque indicating incomplete crystallization. This is contrary to the
345 expected increase in secondary nucleation. However, the evaluation of torque allows only qualitative
346 statements of crystallization process in dispersed systems under mechanical stresses. A combination
347 of optical, mechanical and thermal method to quantify the crystallization behavior of dispersed
348 systems is a subject of our ongoing investigations and will be presented in our following papers.

351 **Author Contributions:** S. Abramov and H. P. Karbstein provided the idea, conceived and designed the
352 experiments; S. Abramov, K. Shah and L. Weißenstein performed the experiments; S. Abramov, K. Shah and L.
353 Weißenstein analyzed the data; S. Abramov wrote the paper; H. P. Karbstein corrected the paper

354 **Conflicts of Interest:** The authors declare no conflict of interest. The funding sponsors had no role in the design
355 of the study; in the collection, analyses, or interpretation of data; in the writing of the manuscript, and in the
356 decision to publish the results.

357 **Appendix A: Droplet size distribution**

358   Droplet size distributions (DSD) of 1wt% alkane dispersions, prepared with the same energy
359 input E_v but at different temperatures (10K above the melting temperature of respectively alkanes),
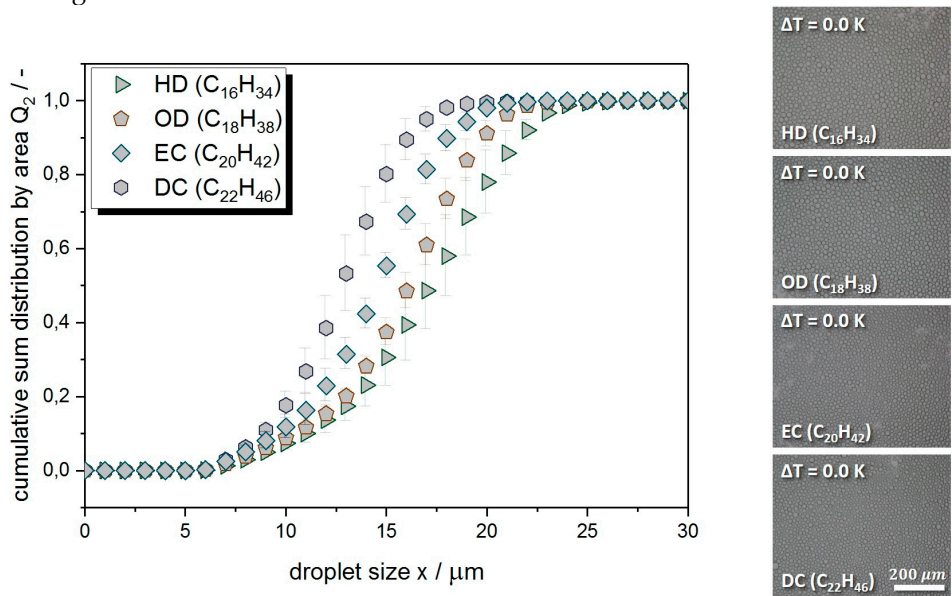360 are shown in Figure A1.

361

362 Figure A1: Cumulative sum distribution by area Q_2 of 1wt% alkane in water emulsions stabilized with
363 1wt% Tween20® and measured at $\vartheta_{m,alkane}$ with PLM/IP. Triangles: DSD of hexadecane dispersions.
364 Pentagons: DSD of octadecane dispersions. Diamonds: DSD of eicosane dispersions. Hexagons: DSD
365 of docosane dispersions. Length of the scale bar is 200 μm.

366   We chose polarizing light microscopy and image processing instead of laser diffraction and
367 dynamic light scattering for the characterization of the DSD to ensure the measurement of only liquid
368 droplets. For this we worked at exact alkane melting temperature during the measurement and were
369 able to detect possible crystalline structures due to polarization. This technique also allowed us to
370 avoid unwanted measurements of agglomerates/aggregates, which might be formed due to colloidal
371 processes in dispersed systems. As we showed in our previous investigations [14, 15] the mean
372 droplet diameter measured with thermo-optical method is almost identical within the standard

373 deviation to the more statistic laser diffraction measurements and will be used as the characteristic
374 size value for further discussions. The mean droplet diameter of the alkane dispersions is given in
375 Table A1.

376 Table A1: Mean droplet diameter $x_{50.2}$ and number of characterized droplets N with standard
377 deviations. Measured with polarizing light microscopy/image processing.

alkane (dispersed phase)	$x_{50.2}$ / μm	N / -
C16: hexadecane (HD)	17.2+/-1.2	1297+/-306
C18: octadecane (OD)	16.1+/-0.4	1653+/-148
C20: eicosane (EC)	14.6+/-0.2	1774+/-65
C22: docosane (DC)	12.8+/-1.0	2506+/-86

378 Applying the same E_v in the emulsification process resulted in different DSDs and $x_{50.2}$ values.
379 The differences are caused by different emulsification temperatures and material properties resulting
380 in different viscosity ratios and interfacial tensions between the dispersed and continuous phase.
381 Both, the viscosity ratio and interfacial tension, influence the emulsification efficiency and thus the
382 final DSD. Consequently, $x_{50.2}$ decreased within the homologous series from 17.2μm (HD, lowest
383 emulsification temperature) to 12.8μm (DC, highest emulsification temperature).

384 **Appendix B: Onset crystallization temperature and melting point**

385 The onset crystallization and melting point in 1wt% dispersions were determined optically using
386 polarized cryo microscopy and are shown in Figure B1, micrographs on the right. Since the
387 crystallization in dispersions is an individual stochastic process the onset crystallization temperature
388 was determined by the first crystallized droplet. The melting temperature was determined by the
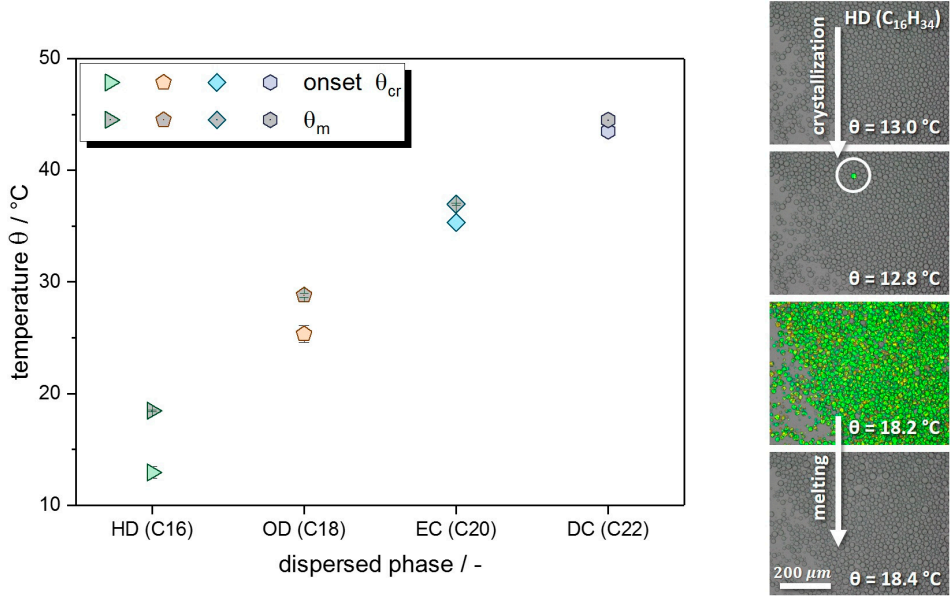389 melting of all crystalline structures within the dispersion.

390

391 Figure B1: Onset crystallization temperature $onset\ \vartheta_{cr,dispersion}$ and melting point/temperature
392 $\vartheta_{m,dispersion}$ of the alkane dispersions. Micrographs on the right show one of three exemplary
393 determination of onset crystallization temperature and melting point in hexadecane dispersions.
394 Length of the scale bar is 200 μm.

395 The melting temperature was always higher, then the onset crystallization. With increasing
396 chain length of the alkanes, the difference between melting temperature and onset crystallization
397 decreased. Consequently, with increasing chain length of the alkanes lower supercooling was

398 required for crystallization in alkane dispersions. Melting temperature and onset crystallization are
399 summarized in Table B2.

400 Table B2: Onset crystallization temperature $onset\ \vartheta_{cr,dispersion}$, melting point/temperature
401 $\vartheta_{m,dispersion}$ of the alkane dispersions and reference melting temperature of the bulk $\vartheta_{m,ref,bulk}$
402 according to [52]

alkane (dispersed phase)	$onset\theta_{cr,dispersion}$/°C	$\theta_{m,dispersion}$/°C	$\theta_{m,ref,bulk}$/°C [52]
C16: hexadecane (HD)	12.9+/-0.5	18.5+/-0.1	18.2
C18: octadecane (OD)	25.3+/-0.8	28.8+/-0.2	28.2
C20: eicosane (EC)	35.3+/-0.2	37.0+/-0.1	36.6
C22: docosane (DC)	43.5+/-0.1	44.5+/-0.0	44.1

403 We compared the melting temperatures of the dispersions with the reference melting
404 temperature of the bulk (data from [52]) and detected differences in the range of 0.5K. Those
405 differences result from the resolution of the method (signal per time unit), the dispersed state (bulk
406 vs. dispersion) and the purity of the substances. In this paper, we therefore refer the melting
407 temperature $\vartheta_{m,alkane}$ or supercooling ΔT to the determined $\vartheta_{m,dispersion}$ using our thermo-optical
408 method.

409 **Appendix C: Time dependency of crystallization process**

410 Nucleation is a time dependent process during the crystallization procedure. Exceeding the
411 driving forces, such as supersaturation and/or supercooling, is usually required to overcome the
412 nucleation barrier and still does not necessarily result in immediate crystallization. The induction
413 time, which is required from certain supercooling/supersaturation to nucleation, differs in
414 dependence of formulation and process. To describe the time dependency on nucleation in alkane
415 dispersions we varied the cooling rate and followed optically the crystallization process (see Figure
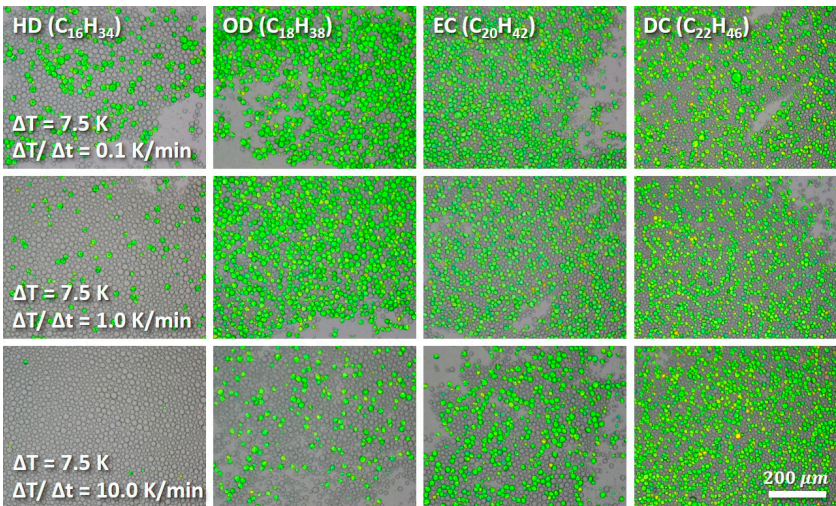416 C1).

418 Figure C1: Micrographs of 1wt% alkane dispersions at ΔT=7.5K during supercooling with different
419 cooling rates. Length of the scale bar is 200 μm.

420 We observed decreasing time dependency of the crystallization in dispersions with increasing
421 chain length from HD(C_{16}) over OD(C_{18}) and EC(C_{20}) to DC(C_{22}). In DC dispersions, the amount of
422 crystallized droplets within triple determination was comparatively equal independent of the cooling
423 rate. EC and OD dispersions showed similar crystallization behavior at low (0.1K/min) and medium
424 (1.0K/min) cooling rates as DC dispersions. At high (10K/min) cooling rate, both EC and OD
425 dispersions, showed a lower number of crystallized droplets. The time dependency at the high

426 cooling rate was higher in OD dispersions than in EC dispersions. In case of HD dispersions, the
427 number of crystallized droplets increased with decreasing cooling rate and showed more time
428 dependent crystallization behavior as OD, EC and DC dispersions. In order to evaluate the time
429 dependency compared to the driving force of supercooling we performed isothermal observations of
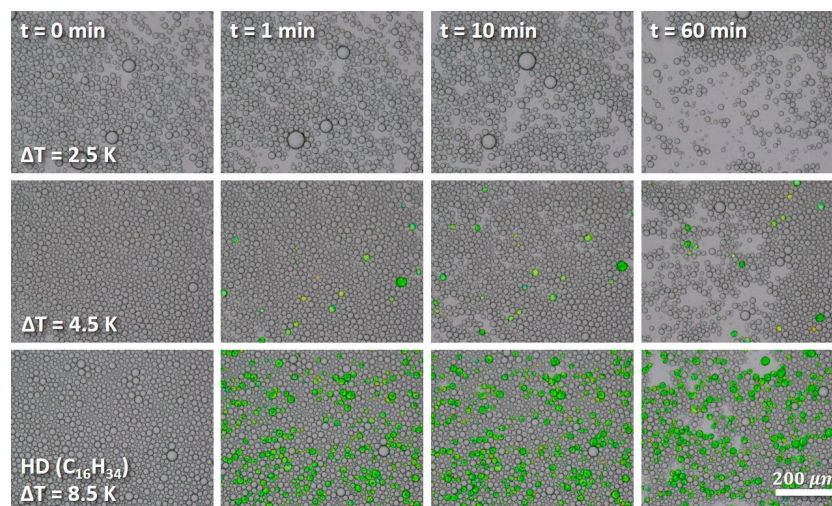430 crystallization in HD dispersions (see Figure C2).

431

432 Figure C2: Micrographs of 1wt% HD dispersions at different supercooling during one-hour
433 isothermal observations. Length of the scale bar is 200 μm

434 During the isothermal observation at low supercooling (ΔT=2.5K) we did not detect any
435 crystallization in HD dispersions within one-hour observation, which corresponds to the onset
436 crystallization investigations in appendix B. Increasing the supercooling (to ΔT=4.5K) led to
437 crystallization of few droplets within one minute. The number of crystallized droplets remained
438 comparatively equal within one-hour observation. At high supercooling (ΔT=8.5K) more droplets
439 crystallized in HD dispersions within one minute. Also here, the number of crystallized droplets did
440 not change within one hour.
441 The influence of supercooling was higher than the time dependency during isothermal
442 observations in HD dispersions with no significant change in number of crystallized droplets after
443 one minute. According to no change in number of crystallized droplets after one minute in HD
444 dispersions and nearly no time dependency in investigated time scale in OD, EC and DC dispersions
445 we chose 1K/min as a cooling rate for further investigations.

446

References

1.   Müller, R.H.; Petersen, R.D.; Hommoss, A.; Pardeike, J. Nanostructured lipid carriers (NLC) in cosmetic dermal products. *Advanced drug delivery reviews* **2007**, *59*, 522–530, doi:10.1016/j.addr.2007.04.012.

2.   Pardeike, J.; Hommoss, A.; Müller, R.H. Lipid nanoparticles (SLN, NLC) in cosmetic and pharmaceutical dermal products. *International journal of pharmaceutics* **2009**, *366*, 170–184, doi:10.1016/j.ijpharm.2008.10.003.

3.   McClements, D.J. Crystals and crystallization in oil-in-water emulsions: implications for emulsion-based delivery systems. *Advances in colloid and interface science* **2012**, *174*, 1–30, doi:10.1016/j.cis.2012.03.002.

4.   Rostami, E.; Kashanian, S.; Azandaryani, A.H.; Faramarzi, H.; Dolatabadi, Jafar Ezzati Nazhad; Omidfar, K. Drug targeting using solid lipid nanoparticles. *Chemistry and physics of lipids* **2014**, *181*, 56–61, doi:10.1016/j.chemphyslip.2014.03.006.

5.   Wissing, S. Cosmetic applications for solid lipid nanoparticles (SLN). *International journal of pharmaceutics* **2003**, *254*, 65–68, doi:10.1016/S0378-5173(02)00684-1.

6.   Müller, R. Solid lipid nanoparticles (SLN) for controlled drug delivery - a review of the state of the art. *European Journal of Pharmaceutics and Biopharmaceutics* **2000**, *50*, 161–177, doi:10.1016/S0939-6411(00)00087-4.

7.   Mehnert, W. Solid lipid nanoparticles Production, characterization and applications. *Advanced drug delivery reviews* **2001**, *47*, 165–196, doi:10.1016/S0169-409X(01)00105-3.

8.   Wissing, S.A.; Kayser, O.; Müller, R.H. Solid lipid nanoparticles for parenteral drug delivery. *Advanced drug delivery reviews* **2004**, *56*, 1257–1272, doi:10.1016/j.addr.2003.12.002.

9.   Coupland, J.N. Crystallization in emulsions. *Current Opinion in Colloid & Interface Science* **2002**, *7*, 445–450, doi:10.1016/S1359-0294(02)00080-8.

10.   Weiss, J.; Decker, E.A.; McClements, D.J.; Kristbergsson, K.; Helgason, T.; Awad, T. Solid Lipid Nanoparticles as Delivery Systems for Bioactive Food Components. *Food Biophysics* **2008**, *3*, 146–154, doi:10.1007/s11483-008-9065-8.

11.   *Emulgiertechnik. Grundlagen, Verfahren und Anwendungen;* Köhler, K.; Schuchmann, H.P., Eds., 3. Aufl.; Behr: Hamburg, 2012.

12.   Walstra, P. *Physical chemistry of foods;* Marcel Dekker: New York, 2003.

13.   Köhler, K.; Hensel, A.; Kraut, M.; Schuchmann, H.P. Melt emulsification—Is there a chance to produce particles without additives? *Particuology* **2011**, *9*, 506–509, doi:10.1016/j.partic.2011.03.009.

14.   Abramov, S.; Ruppik, P.; Schuchmann, H. Crystallization in Emulsions: A Thermo-Optical Method to Determine Single Crystallization Events in Droplet Clusters. *Processes* **2016**, *4*, 25, doi:10.3390/pr4030025.

15.   Abramov, S.; Berndt, A.; Georgieva, K.; Ruppik, P.; Schuchmann, H.P. Investigation of the influence of mean droplet size and shear rate on crystallization behavior of hexadecane-in-water dispersions. *Colloids and Surfaces A: Physicochemical and Engineering Aspects* **2017**, *529*, 513–522, doi:10.1016/j.colsurfa.2017.06.029.

16.   Tippetts, M.; Martini, S. Effect of cooling rate on lipid crystallization in oil-in-water emulsions. *Food Research International* **2009**, *42*, 847–855, doi:10.1016/j.foodres.2009.03.009.

17.   Bolzinger, M.A.; Cogne, C.; Lafferrere, L.; Salvatori, F.; Ardaud, P.; Zanetti, M.; Puel, F. Effects of surfactants on crystallization of ethylene glycol distearate in oil-in-water emulsion. *Colloids and Surfaces A: Physicochemical and Engineering Aspects* **2007**, *299*, 93–100, doi:10.1016/j.colsurfa.2006.11.026.

18.   Ghosh, S.; Cramp, G.L.; Coupland, J.N. Effect of aqueous composition on the freeze-thaw stability of emulsions. *Colloids and Surfaces A: Physicochemical and Engineering Aspects* **2006**, *272*, 82–88, doi:10.1016/j.colsurfa.2005.07.013.

19.   Samtlebe, M.; Yucel, U.; Weiss, J.; Coupland, J.N. Stability of Solid Lipid Nanoparticles in the Presence of Liquid Oil Emulsions. *J Am Oil Chem Soc* **2012**, *89*, 609–617, doi:10.1007/s11746-011-1944-3.

20.   Vanapalli, S.A.; Palanuwech, J.; Coupland, J.N. Stability of emulsions to dispersed phase crystallization: effect of oil type, dispersed phase volume fraction, and cooling rate. *Colloids and Surfaces A: Physicochemical and Engineering Aspects* **2002**, *204*, 227–237, doi:10.1016/S0927-7757(01)01135-9.

21.   Vanapalli, S.A.; Palanuwech, J.; Coupland, J.N. Influence of Fat Crystallization on the Stability of Flocculated Emulsions. *J. Agric. Food Chem.* **2002**, *50*, 5224–5228, doi:10.1021/jf020319y.

22.   Ghosh, S.; Rousseau, D. Fat crystals and water-in-oil emulsion stability. *Current Opinion in Colloid & Interface Science* **2011**, *16*, 421–431, doi:10.1016/j.cocis.2011.06.006.

499   23.   Helgason, T.; Awad, T.S.; Kristbergsson, K.; McClements, D.J.; Weiss, J. Influence of Polymorphic
500   Transformations on Gelation of Tripalmitin Solid Lipid Nanoparticle Suspensions. *J Am Oil Chem Soc* **2008**,
501   *85*, 501–511, doi:10.1007/s11746-008-1219-9.
502   24.   Yang, D.; Hrymak, A.N. Crystal Morphology of Hydrogenated Castor Oil in the Crystallization of
503   Oil-in-Water Emulsions: Part I. Effect of Temperature. *Ind. Eng. Chem. Res.* **2011**, *50*, 11585–11593,
504   doi:10.1021/ie1025985.
505   25.   Povey, M.J.W. Crystal nucleation in food colloids. *Food Hydrocolloids* **2014**, *42*, 118–129,
506   doi:10.1016/j.foodhyd.2014.01.016.
507   26.   Rousseau, D. Fat crystals and emulsion stability — a review. *Food Research International* **2000**, *33*, 3–14,
508   doi:10.1016/S0963-9969(00)00017-X.
509   27.   Himawan, C.; Starov, V.M.; Stapley, A G F. Thermodynamic and kinetic aspects of fat crystallization.
510   *Advances in colloid and interface science* **2006**, *122*, 3–33, doi:10.1016/j.cis.2006.06.016.
511   28.   Kashchiev, D.; van Rosmalen, G.M. Review: Nucleation in solutions revisited. *Cryst. Res. Technol.* **2003**,
512   *38*, 555–574, doi:10.1002/crat.200310070.
513   29.   Hindle; Povey; Smith. Kinetics of Crystallization in n-Hexadecane and Cocoa Butter Oil-in-Water
514   Emulsions Accounting for Droplet Collision-Mediated Nucleation. *Journal of colloid and interface science* **2000**,
515   *232*, 370–380, doi:10.1006/jcis.2000.7174.
516   30.   Dickinson, E.; Ma, J.; Povey, Malcolm J. W. Crystallization kinetics in oil-in-water emulsions
517   containing a mixture of solid and liquid droplets. *Faraday Trans.* **1996**, *92*, 1213, doi:10.1039/FT9969201213.
518   31.   Petersen, S.; Ulrich, J. Role of Emulsifiers in Emulsion Technology and Emulsion Crystallization.
519   *Chem. Eng. Technol.* **2013**, *36*, 398–402, doi:10.1002/ceat.201200648.
520   32.   Kim, J.-W.; Ulrich, J. Prediction of degree of deformation and crystallization time of molten droplets
521   in pastillation process. *International journal of pharmaceutics* **2003**, *257*, 205–215, doi:10.1016/S0378-
522   5173(03)00141-8.
523   33.   Helgason, T.; Awad, T.S.; Kristbergsson, K.; McClements, D.J.; Weiss, J. Effect of surfactant surface
524   coverage on formation of solid lipid nanoparticles (SLN). *Journal of colloid and interface science* **2009**, *334*, 75–
525   81, doi:10.1016/j.jcis.2009.03.012.
526   34.   McClements, D.J.; Dungan, S.R.; GERMAN, J.B.; SIMONEAU, C.; KINSELLA, J.E. Droplet Size and
527   Emulsifier Type Affect Crystallization and Melting of Hydrocarbon-in-Water Emulsions. *J Food Science* **1993**,
528   *58*, 1148–1151, doi:10.1111/j.1365-2621.1993.tb06135.x.
529   35.   Ruecroft, G.; Hipkiss, D.; Ly, T.; Maxted, N.; Cains, P.W. Sonocrystallization: The Use of Ultrasound
530   for Improved Industrial Crystallization. *Org. Process Res. Dev.* **2005**, *9*, 923–932, doi:10.1021/op050109x.
531   36.   Alexander, A.J.; Camp, P.J. Single Pulse, Single Crystal Laser-Induced Nucleation of Potassium
532   Chloride. *Crystal Growth & Design* **2009**, *9*, 958–963, doi:10.1021/cg8007415.
533   37.   Javid, N.; Kendall, T.; Burns, I.S.; Sefcik, J. Filtration Suppresses Laser-Induced Nucleation of Glycine
534   in Aqueous Solutions. *Crystal Growth & Design* **2016**, *16*, 4196–4202, doi:10.1021/acs.cgd.6b00046.
535   38.   Da Pieve, S.; Calligaris, S.; Co, E.; Nicoli, M.C.; Marangoni, A.G. Shear Nanostructuring of
536   Monoglyceride Organogels. *Food Biophysics* **2010**, *5*, 211–217, doi:10.1007/s11483-010-9162-3.
537   39.   Garbolino, C.; Ziegler, G.R.; Coupland, J.N. Ultrasonic determination of the effect of shear on lipid
538   crystallization. *J Amer Oil Chem Soc* **2000**, *77*, 157–162, doi:10.1007/s11746-000-0025-5.
539   40.   Saggin, R.; Coupland, J.N. Shear and longitudinal ultrasonic measurements of solid fat dispersions. *J
540   Amer Oil Chem Soc* **2004**, *81*, 27–32, doi:10.1007/s11746-004-0854-2.
541   41.   Sonwai, S.; Mackley, M.R. The effect of shear on the crystallization of cocoa butter. *J Amer Oil Chem
542   Soc* **2006**, *83*, 583–596, doi:10.1007/s11746-006-1243-6.
543   42.   Tarabukina, E.; Jego, F.; Haudin, J.-M.; Navard, P.; Peuvrel-Disdier, E. Effect of shear on the rheology
544   and crystallization of palm oil. *Journal of food science* **2009**, *74*, 16, doi:10.1111/j.1750-3841.2009.01304.x.
545   43.   Vanapalli, S.A.; Coupland, J.N. Emulsions under shear—the formation and properties of partially
546   coalesced lipid structures. *Food Hydrocolloids* **2001**, *15*, 507–512, doi:10.1016/S0268-005X(01)00057-1.
547   44.   Barfod, N.M.; Krog, N. Destabilization and fat crystallization of whippable emulsions (toppings)
548   studied by pulsed NMR. *J Am Oil Chem Soc* **1987**, *64*, 112–119, doi:10.1007/BF02546264.
549   45.   Goff, H.D. Instability and Partial Coalescence in Whippable Dairy Emulsions. *Journal of Dairy Science*
550   **1997**, *80*, 2620–2630, doi:10.3168/jds.S0022-0302(97)76219-2.
551   46.   Stapley, A.G.F.; Tewkesbury, H.; Fryer, P.J. The effects of shear and temperature history on the
552   crystallization of chocolate. *J Amer Oil Chem Soc* **1999**, *76*, 677–685, doi:10.1007/s11746-999-0159-3.

553   47.   Hindle, S.A.; Povey, Malcolm J. W.; Smith, K.W. Characterizing cocoa butter seed crystals by the oil-
554   in-water emulsion crystallization method. *J Amer Oil Chem Soc* **2002**, *79*, 993–1002, doi:10.1007/s11746-002-
555   0593-4.
556   48.   Sir William Thomson. On the equilibrium of vapor at a curved surface of liquid. *Philosophical Magazine*
557   **1871**, 448–452.
558   49.   Povey, M.J.W. Crystal nucleation in food colloids. *Food Hydrocolloids* **2014**, *42*, 118–129,
559   doi:10.1016/j.foodhyd.2014.01.016.
560   50.   Pound, G.M.; La Mer, V.K. Kinetics of Crystalline Nucleus Formation in Supercooled Liquid Tin 1,2.
561   *J. Am. Chem. Soc.* **1952**, *74*, 2323–2332, doi:10.1021/ja01129a044.
562   51.   Rodriguez-Spong, B.; Price, C.P.; Jayasankar, A.; Matzger, A.J.; Rodriguez-Hornedo, N. General
563   principles of pharmaceutical solid polymorphism: a supramolecular perspective. *Advanced drug delivery*
564   *reviews* **2004**, *56*, 241–274, doi:10.1016/j.addr.2003.10.005.
565   52.   Domalski, E.S.; Hearing, E.D. Heat Capacities and Entropies of Organic Compounds in the
566   Condensed Phase. Volume III. *J. Phys. Chem. Ref. Data* **1996**, *25*, 1–525, doi:10.1021/ja01129a044.